

A DYNAMICAL CONSTRAINT ON INTERSTELLAR DUST MODELS FROM RADIATIVE TORQUE DISRUPTION

THIEM HOANG^{1,2}

¹ Korea Astronomy and Space Science Institute, Daejeon 34055, South Korea; thiemhoang@kasi.re.kr
 and

² Korea University of Science and Technology, 217 Gajeong-ro, Yuseong-gu, Daejeon, 34113, South Korea

ABSTRACT

Interstellar dust is an essential component of the interstellar medium (ISM) and plays critical roles in astrophysics. Achieving an accurate model of interstellar dust is therefore of great importance. Interstellar dust models are usually built based on observational constraints such as starlight extinction and polarization, but dynamical constraints such as grain rotation are not considered. In this paper, we show that a newly discovered effect by Hoang et al., so-called Radiative Torque Disruption (RATD), due to centrifugal stress within suprathermally rotating grains can act as an important dynamical constraint for dust models. Using this dynamical constraint, we will derive the maximum size of grains that can survive in the ISM for four different dust models, including a contact binary, a composite grain, a silicate-core and icy amorphous carbon mantle, and compact model for the different radiation fields. We find that the different dust models have the different maximum size due to their different tensile strengths, and the largest maximum size corresponds to compact grains with a highest tensile strength. We show that the composite grain model cannot be ruled out if constituent particles are very small with radius $a_p \leq 25$ nm, but large composite grains would be destroyed if the particles are large with $a_p \geq 50$ nm. Finally, we suggest that grain internal structures can be constrained with observational data by using the dynamical RATD constraint.

Keywords: ISM: dust-extinction, ISM: general, radiation: dynamics, polarization, magnetic fields

1. INTRODUCTION

Interstellar dust is an essential component of the interstellar medium (ISM) and plays critical roles in astrophysics, including star and planet formation, grain chemistry, and being a tracer of magnetic fields. Observation of starlight extinction and polarization combined with spectroscopic observations reveal that interstellar dust includes two major components, silicate and carbonaceous materials (see [Draine 2003](#) for a complete review) and have different sizes and non-spherical shapes. As a result, constructing a standard model for interstellar dust is a fundamental scientific task, and it has vast application for many sub-fields of astrophysics.

An interstellar dust model must include three ingredients: grain composition, grain geometry (shape and internal structure), and grain size distribution. Currently, there are three popular models of interstellar dust. The first dust model assumes two separate components of silicate and carbonaceous materials and can reproduce wavelength-dependence extinction ([Mathis et al. 1977](#); [Draine & Lee 1984](#)). Later, an additional ultrasmall carbonaceous grains, namely polycyclic aromatic carbons

(PAHs) is introduced to become PAH-silicate-graphite model ([Draine & Li 2007](#)). The second, composite grain model is introduced by [Mathis & Whiffen \(1989\)](#) in which the grain consists of both silicate and carbonaceous particles loosely bounded together by adhesion forces. The third, core-mantle model comprises a silicate core and amorphous carbonaceous mantle ([Greenberg & Li 1996](#); [Jones et al. 2013](#)). Although the PAH-silicate-graphite model is widely used in astrophysics, a remaining question raised in [Draine \(2003\)](#) is "Are there really separate populations of carbonaceous grains and silicate grains? If so, how does grain growth in the ISM maintain these separate populations?"

An accurate model for interstellar dust is of great importance for developing an accurate foreground polarization model, which is urgently needed for precise detection of Cosmic Microwave Background (CMB) B-mode signal (see [Kamionkowski & Kovetz 2016](#) for a review). Currently, all polarized foreground models assume two distinct dust components ([Draine & Fraisse 2009](#); [Guillet et al. 2017](#); [Hensley & Bull 2018](#)). Yet it is known that a model with mixed silicate and amorphous carbon

materials would produce different polarization spectra, resulting in the frequency degeneracy (see e.g., [Guillet et al. 2017](#)).

Silicate and carbonaceous grains are formed from distinct environments, with the former dust being formed in the envelope of O-rich Asymptotic Giant Branch (AGB) stars and the later one being formed in the envelope of C-rich AGB stars. Intuitively, it is hard to believe that these two populations are completely separate in the ISM because mixing can naturally occur during the grain growth process in the ISM which is thought to be a dominant source of interstellar dust.

Polarimetric observations are particularly useful to differentiate grain models. [Chiar et al. \(2006\)](#) found that the $3.4\ \mu\text{m}$ C-H feature is negligibly polarized, whereas the $9.7\ \mu\text{m}$ Si-O feature is strongly polarized ([Aitken et al. 1988](#)) for the light of sights toward the Galactic Center. The authors suggest that carbonaceous grains must be a separate component and these grains should be not aligned. Theoretically, if carbon grains are separate, they cannot be aligned due to diamagnetic nature of these dust component ([Hoang & Lazarian 2016](#)). If silicate and carbonaceous components are separate as suggested by the non-detection of $3.4\ \mu\text{m}$ C-H polarization, then, what physical mechanism prevents such a mixed grain model to exist in the ISM?

A standard procedure in constructing a dust model based on observational constraints is varying the grain size distribution to achieve the best-fit model ([Mathis et al. 1977](#); [Kim et al. 1994](#); [Zubko et al. 2004](#); [Draine & Fraisse 2009](#); [Hoang 2017](#)). While the lower cutoff of the size distribution is physically determined by thermal sublimation of nanoparticles ([Guhathakurta & Draine 1989](#)), the upper cutoff is a free parameter in the dust models.

[Hoang et al. \(2018b\)](#) discovered that large dust grains can be completely disrupted when the centrifugal stress induced by suprathermal rotation driven by radiative torques (RATs; [Draine & Weingartner 1996](#); [Hoang & Lazarian 2008](#); [Hoang & Lazarian 2009](#)) exceeds the maximum tensile stress (i.e., tensile strength) of dust grains.¹ Because the efficiency of radiative torque disruption (RATD) mechanism depends on the radiation intensity and the grain tensile strength which is determined by grain internal structures (i.e., grain model), the upper cutoff of the grain size distribution cannot be a free parameter. It should be *dynamically* related to the internal structure and ambient conditions. The goal of this paper is to introduce a *dynamical constraint*

for dust models using the RATD mechanism and to explore its potential application for probing grain internal structures with observations.

The structure of the paper is as follows. In Section 2 we will describe three popular dust models and calculate their tensile strengths. Section 3 is devoted to calculate rotation rate of grains by radiative torques. We will derive the critical grain size for rotational disruption for the different dust models in Section 4. In Section 5 we discuss the importance of the introduced dynamical constraint for the different dust models and the possibility of probing internal structures of dust grains with observations combined with RATD effect. A summary of our main findings is given in Section 6.

2. DUST MODELS AND TENSILE STRENGTH

2.1. Contact binary model

We first consider a possible scenario in which a compact silicate particle collides with a carbonaceous particle in the ISM to form a contact binary grain. Upon collision, two particles make a contact area, as shown in Figure 1 (model a).

The physics of contact solids is well studied in literature ([Johnson et al. 1971](#)). The underlying physics is as follows. When two solid spheres are in contact, van der Waals forces tend to pull two spheres together. At the same time, repulsive force between nuclei act to push them. The equilibrium is established when the attractive force is equal to repulsive force. As a result, a common volume of circular area with radius a_0 is established, with the value a_0 depending on materials ([Chokshi et al. 1993](#); [Dominik & Tielens 1997](#)). The adhesive force due to the contact is calculated using the model of [Johnson et al. \(1971\)](#) (i.e., JKR model; see also [Heim et al. 1999](#)):

$$F_{\text{JKR}} = 3\pi R\gamma, \quad (1)$$

where γ is the surface energy per unit area of the material, and $R = R_1 R_2 / (R_1 + R_2)$ is the sphere radii. The value of γ is given by

$$\gamma = \gamma_1 + \gamma_2 - 2\gamma_{12}, \quad (2)$$

where γ_{12} is the interface energy. For similar materials, $\gamma_1 = \gamma_2$ and $\gamma_{12} = 0$. The surface energy value varies from $\gamma = 10 - 25\ \text{erg cm}^{-2}$ ([Heim et al. 1999](#)).

The interaction force can be rewritten as

$$F_{\text{JKR}} \simeq 10^{-3} \gamma_1 R_{-5}\ \text{dyne}, \quad (3)$$

where $\gamma_1 = (\gamma/10\ \text{dyn cm}^{-2})$, $R_{-5} = R/10^{-5}\ \text{cm}$. The force F_{JKR} is the same as the pull-off force F_c that is required to pull two spheres apart.

Let $R_2 = sR_1$ with $s \leq 1$. Let a be the effective grain size, which is defined as the radius of the equivalent

¹ The rotational disruption can also work for nanoparticles that are spun-up to suprathermal rotation by supersonic neutral drift in C-shocks ([Hoang & Tram 2018](#)).

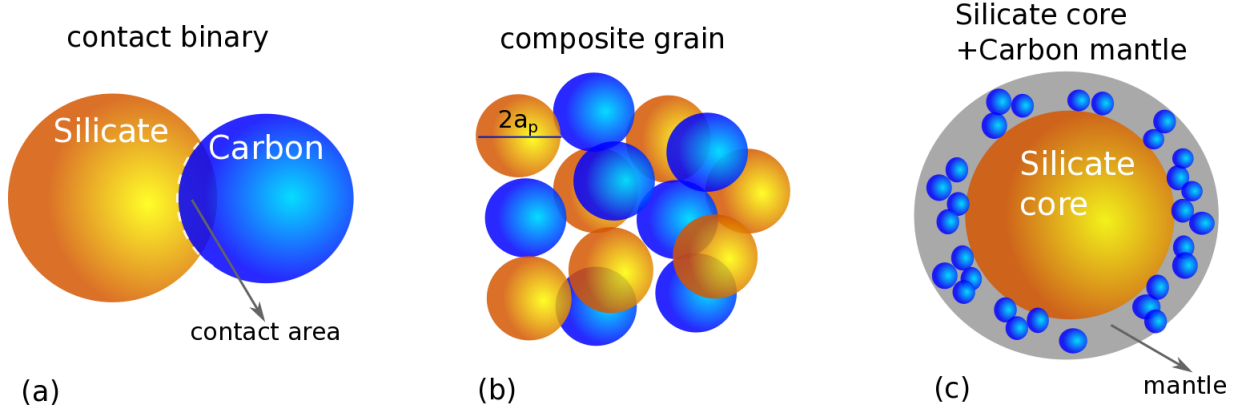


Figure 1. Schematic illustration of three different grain models that form from mixing of silicate and carbonaceous grains: (a) Contact binary grain model of a spherical silicate core in contact with a carbonaceous particle, (b) A composite grain consisting of many individual particles of silicate and carbonaceous materials, (c) A silicate core and carbon icy mantle model.

sphere of the same volume. Then, one obtains

$$a \sim R_1^2 + R_2^3 = R_1^3(1 + s^3), \quad (4)$$

where the contact area is small compared to the grain size.

2.2. Composite grain model

We now consider a composite grain model as proposed by Mathis & Whiffen (1989). This composite model relies on the fact that upon entering the ISM, original silicate and carbonaceous grains are shattered (e.g., by shocks) into small fragments. The subsequent collisions of these fragments reform interstellar composite grains. Following Mathis & Whiffen (1989), individual particles are assumed to be compact and spherical of radius a_p .² Particles can be of silicate or carbonaceous materials. Let P be the porosity which is defined such that the mass density of the porous grain is $\rho = \rho_0(1 - P)$ with ρ_0 being the mass density of fully compact grain. The value $P = 0.2$ indicates an empty volume of 20%.

To calculate the tensile strength of a composite grain, we follow the approach in Greenberg et al. (1995) where the particle is assumed to have a icy mantle, which is plausible because grain coagulation by grain-grain collisions is expected in cold environments such as outflows.

Let \bar{E} be the mean intermolecular interaction energy at the contact surface between two particles and h be the mean intermolecular distance at the contact surface. Let β be the mean number of contact points per particle between 1-10. The volume of interaction region is $V_{int} = (2ha_p^2)$. Following Greenberg et al. (1995), one can estimate the tensile strength as given by the volume

density of interaction energy

$$S_{\max} = 3\beta(1 - P) \frac{\bar{E}}{2ha_p^2}. \quad (5)$$

Assuming that the interaction between contact particles is only van der Waals forces, thus one can write $\bar{E} = \alpha 10^{-3}$ eV where α is the coefficient of order of unity (see e.g., Li & Greenberg 1997). The tensile strength can be rewritten as

$$S_{\max} \simeq 1.6 \times 10^6 \left(\frac{\beta}{5}\right) (1 - P) \left(\frac{\alpha \bar{E}}{10^{-3} \text{eV}}\right) \times \left(\frac{a}{5 \text{nm}}\right)^{-2} \left(\frac{0.3 \text{nm}}{h}\right) \text{ erg cm}^{-3}. \quad (6)$$

The tensile strength decreases rapidly with increasing the particle radius, as a_p^{-2} , and decreases with increasing the porosity P . In the following, we fix the porosity $P = 0.2$, as previously assumed for *Planck* data modeling (Guillet et al. 2017).

2.3. Silicate-core and amorphous carbon mantle grain model

Finally, we consider a simple grain model including amorphous silicate core and carbonaceous material in the form of small grains or mantle (see Figure 1, model c). Let R_1 be the radius of silicate core and L be the thickness of the mantle. The effective grain size for this model is $a = R_1 + L$.

For the case of pure ice mantle, one can take the tensile strength of bulk ice $S_{\max} \sim 10^7$ erg cm⁻³ for the mantle layer. In the presence of small amorphous carbon grains, the tensile strength of the mantle layer might be increased considerably by several times (Litwin et al. 2012).

The silicate core can be either compact or composite, but their nature is not important for the destruction of the mantle layer because even the bonds in the composite core are broken by the centrifugal force,

² In realistic conditions, one cannot have the same size a_p because of grain-grain collisions of different sizes. For the sake of simplicity without losing the underlying physics, we approximate the particles to have an average size.

the grain is only destroyed when the outer layer is ejected. Thus, we assume that the core is compact with $S_{\text{max}} \sim 10^9 - 10^{10} \text{ erg cm}^{-3}$.

3. GRAIN SUPRATHERMAL ROTATION BY RADIATIVE TORQUES

3.1. Radiative torques for irregular grains

Let u_λ be the spectral energy density of radiation field at wavelength λ . The energy density of the radiation field is then $u_{\text{rad}} = \int u_\lambda d\lambda$. To describe the strength of a radiation field, let define $U = u_{\text{rad}}/u_{\text{ISRF}}$ with $u_{\text{ISRF}} = 8.64 \times 10^{-13} \text{ erg cm}^{-3}$ being the energy density of the average interstellar radiation field (ISRF) in the solar neighborhood as given by Mathis et al. (1983). Thus, the typical value for the ISRF is $U = 1$.

Radiative torque (RAT) arising from the interaction of an anisotropic radiation field with an irregular grain is defined as

$$\Gamma_\lambda = \pi a^2 \gamma_{\text{rad}} u_\lambda \left(\frac{\lambda}{2\pi} \right) Q_\Gamma, \quad (7)$$

where γ_{rad} is the anisotropy degree of the radiation field, Q_Γ is the RAT efficiency, and a is the effective size of the grain which is defined as the radius of the sphere with the same volume as the irregular grain (Draine & Weingartner 1996; Lazarian & Hoang 2007).

The magnitude of RAT efficiency, Q_Γ can be approximated by a power-law (Hoang & Lazarian 2008):

$$Q_\Gamma \sim 0.4 \left(\frac{\lambda}{1.8a} \right)^\eta, \quad (8)$$

where $\eta = 0$ for $\lambda \leq 1.8a$ and $\eta = -3$ for $\lambda > 1.8a$.

Numerical calculations of RATs for several shapes of different optical constants in Lazarian & Hoang (2007) find the slight difference in RATs among the realization. An extensive study for a large number of irregular shapes by Herranen et al. (2018) shows little difference in RATs for silicate, carbonaceous, and iron compositions. Moreover, the analytical formula (Eq. 8) is also in a good agreement with their numerical calculations. Therefore, one can use Equation (8) for the different grain compositions and grain shapes, and the difference is an order of unity

Let $\bar{\lambda} = \int \lambda u_\lambda d\lambda / u_{\text{rad}}$ be the mean wavelength of the radiation field. For the ISRF, $\bar{\lambda} = 1.2 \mu\text{m}$. The average radiative torque efficiency over the spectrum is defined as

$$\bar{Q}_\Gamma = \frac{\int \lambda Q_\Gamma u_\lambda d\lambda}{\int \lambda u_\lambda d\lambda}. \quad (9)$$

For interstellar grains with $a \leq \bar{\lambda}/1.8$, \bar{Q}_Γ can be approximated to (Hoang & Lazarian 2014)

$$\bar{Q}_\Gamma \simeq 2 \left(\frac{\bar{\lambda}}{a} \right)^{-2.7} \simeq 2.6 \times 10^{-2} \left(\frac{\bar{\lambda}}{0.5 \mu\text{m}} \right)^{-2.7} a_{-5}^{2.7} \quad (10)$$

where $a_{-5} = a/10^{-5} \text{ cm}$, and $\bar{Q}_\Gamma \sim 0.4$ for $a > \bar{\lambda}/1.8$.

Therefore, for $a \leq \bar{\lambda}/1.8$, the average radiative torque can be given by

$$\begin{aligned} \Gamma_{\text{RAT}} &= \pi a^2 \gamma_{\text{rad}} \left(\frac{\bar{\lambda}}{2\pi} \right) \bar{Q}_\Gamma \\ &\simeq 5.8 \times 10^{-29} a_{-5}^{4.7} \gamma_{\text{rad}} U \bar{\lambda}_{0.5}^{-1.7} \text{ erg}, \end{aligned} \quad (11)$$

where $\bar{\lambda}_{0.5} = \bar{\lambda}/0.5 \mu\text{m}$.

The well-known damping process for a rotating grain is sticking collision with gas atoms, followed by evaporation. Thus, for a gas with He of 10% abundance, the characteristic damping time is

$$\begin{aligned} \tau_{\text{gas}} &= \frac{3}{4\sqrt{\pi}} \frac{I}{1.2 n_{\text{H}} m_{\text{H}} v_{\text{th}} a^4} \\ &\simeq 8.74 \times 10^4 a_{-5} \hat{\rho} \left(\frac{30 \text{ cm}^{-3}}{n_{\text{H}}} \right) \left(\frac{100 \text{ K}}{T_{\text{gas}}} \right)^{1/2} \text{ yr}, \end{aligned} \quad (12)$$

where $\hat{\rho} = \rho/3 \text{ g cm}^{-3}$ with ρ being the dust mass density, $v_{\text{th}} = (2k_{\text{B}}T_{\text{gas}}/m_{\text{H}})^{1/2}$ is the thermal velocity of a gas atom of mass m_{H} in a plasma with temperature T_{gas} and density n_{H} , the spherical grains are assumed (Hoang & Lazarian 2009; Draine & Weingartner 1996). This time is equal to the time required for the grain to collide with an amount of gas of the grain mass.

IR photons emitted by the grain carry away part of the grain's angular momentum, resulting in the damping of the grain rotation. For strong radiation fields or not very small sizes, grains can achieve equilibrium temperature, such that the IR damping coefficient (see Draine & Lazarian 1998) can be calculated as

$$F_{\text{IR}} \simeq \left(\frac{0.4U^{2/3}}{a_{-5}} \right) \left(\frac{30 \text{ cm}^{-3}}{n_{\text{H}}} \right) \left(\frac{100 \text{ K}}{T_{\text{gas}}} \right)^{1/2}. \quad (13)$$

Other rotational damping processes include plasma drag, ion collisions, and electric dipole emission. These processes are mostly important for PAHs and very small grains (Draine & Lazarian 1998; Hoang et al. 2010; Hoang et al. 2011). Thus, the total rotational damping rate by gas collisions and IR emission can be written as

$$\tau_{\text{damp}}^{-1} = \tau_{\text{gas}}^{-1} (1 + F_{\text{IR}}). \quad (14)$$

For strong radiation fields of $U \gg 1$ and not very dense gas, one has $F_{\text{IR}} \gg 1$. Therefore, $\tau_{\text{damp}} \sim \tau_{\text{gas}}/F_{\text{IR}} \sim a_{-5}^2 U^{2/3}$, which does not depend on the gas properties. In this case, the only damping process is IR emission.

For the radiation source with stable luminosity considered in this paper, radiative torques Γ_{RAT} is constant, and the grain velocity is steadily increased over time. The equilibrium rotation can be achieved at (see Lazarian & Hoang 2007; Hoang & Lazarian 2009; Hoang &

Lazarian 2014):

$$\omega_{\text{RAT}} = \frac{\Gamma_{\text{RAT}} \tau_{\text{damp}}}{I}, \quad (15)$$

where $I = 8\pi\rho a^5/15$ is the grain inertia moment.

3.2. Strong radiation field

For the case with $U \gg 1$, such as $F_{\text{IR}} \gg 1$, plugging Γ_{RAT} (Eq. 7) and τ_{damp} (Eq. 14) into the above equation, one obtain

$$\omega_{\text{RAT}} \simeq 7.1 \times 10^7 \gamma_{\text{rad},-1} a_{-5}^{1.7} U^{1/3} \bar{\lambda}_{0.5}^{-1.7} \text{ Hz}, \quad (16)$$

for grains with $a \leq \bar{\lambda}/1.8$, and

$$\omega_{\text{RAT}} \simeq \frac{1.1 \times 10^9 \gamma}{a_{-5}} U^{1/3} \bar{\lambda}_{0.5}^{-1.7} \text{ Hz}, \quad (17)$$

for grains with $a > \bar{\lambda}/1.8$.

3.3. Weak radiation field

In this case, both gas damping and IR emission is important. The rotation rate by RATs is given by

$$\omega_{\text{RAT}} \simeq 3.2 \times 10^7 \gamma_{\text{rad},-1} a_{-5}^{0.7} U \bar{\lambda}_{0.5}^{-1.7} \times \left(\frac{\hat{n}^{-1} \hat{T}_{\text{gas}}^{-1/2}}{1 + F_{\text{IR}}} \right) \text{ rad s}^{-1}, \quad (18)$$

for grains with $a \leq \bar{\lambda}/1.8$, and

$$\omega_{\text{RAT}} \simeq 1.6 \times 10^8 \frac{\gamma_{-1}}{a_{-5}} U \bar{\lambda}_{0.5}^{-1.7} \times \left(\frac{\hat{n}^{-1} \hat{T}_{\text{gas}}^{-1/2}}{1 + F_{\text{IR}}} \right) \text{ rad s}^{-1}, \quad (19)$$

for grains with $a > \bar{\lambda}/1.8$. Here $\gamma_{\text{rad},-1} = \gamma_{\text{rad}}/0.1$ is the anisotropy of radiation field relative to the typical anisotropy of the diffuse interstellar radiation field.

4. MAXIMUM GRAIN SIZE CONSTRAINED BY RADIATIVE TORQUE DISRUPTION

In this section, we will quantify the effect of centrifugal force due to suprathermal rotation by RATs on grain properties. We consider a range of the radiation strength from $U \sim 0.1 - 1000$. The anisotropy degree also varies with the location, between $\gamma \sim 0.1$ for the diffuse medium to $\gamma \sim 0.7$ for molecular clouds (Bethell et al. 2007), and $\gamma = 1$ for grains close to a star. For numerical estimates below, we will assume an average value of $\gamma = 0.5$, which is realistic for radiation on a cloud surface.

4.1. Contact binary model

The centrifugal force acting on the secondary grain of mass M_2 due to the rotation is

$$F_{\text{Cen}} = M_2 r_2 \omega^2, \quad (20)$$

where r_2 is the distance from the center of M_2 to the grain center of mass, as given by

$$r_2 = \frac{M_1(R_1 + R_2)}{M_1 + M_2} = \frac{\rho_1 R_1(1 + s)}{(\rho_1 + \rho_2 s^3)}, \quad (21)$$

with $r_1 + r_2 \approx R_1 + R_2 = R_1(1 + s)$.

From Equation (20) with Equation (3), one can derive the critical rotation rate required to disrupt the binary grain as follows

$$\omega^2 \geq \omega_{\text{disr}}^2 = \frac{9\gamma(\rho_1 + \rho_2 s^3)}{4(1 + s^2)s^2 \rho_1 \rho_2} \frac{1 + s^3}{a^3}. \quad (22)$$

For $\rho_1 \sim \rho_2 = 3 \text{ g cm}^{-3}$, one obtains

$$\omega_{\text{disr}} \simeq 8.6 \times 10^7 \gamma_1 \frac{(1 + s^3)}{s(1 + s)} a_{-5}^{-3/2} \text{ rad s}^{-1}. \quad (23)$$

Using ω_{RAT} from Equation (18), one can calculate the the disruption size:

$$\left(\frac{a_{\text{disr}}}{0.1 \mu\text{m}} \right)^{3.2} \simeq 1.2 U^{-1/3} \bar{\lambda}_{0.5}^{1.7} \frac{\gamma_1}{\gamma_{\text{rad},-1}} \frac{(1 + s^3)}{s(1 + s)} \quad (24)$$

for strong radiation fields with $F_{\text{IR}} \gg 1$, and

$$\left(\frac{a_{\text{disr}}}{0.1 \mu\text{m}} \right)^{2.2} \simeq 2.6 U^{-1} \bar{\lambda}_{0.5}^{1.7} \frac{\gamma_1}{\gamma_{\text{rad},-1}} \frac{(1 + s^3)}{s(1 + s)} \times \left(\frac{1 + F_{\text{IR}}}{\hat{n}^{-1} \hat{T}_{\text{gas}}^{-1/2}} \right) \quad (25)$$

for arbitrary radiation fields. The disruption size a_{disr} is a maximum grain size a_{max} that suprathermally rotating grains can withstand the rotational disruption by RATs.

Table 1 shows the disruption size for the different radiation strengths and gas density for a binary grain consisting of two identical spheres. Grains larger than $0.15 \mu\text{m}$ cannot be present in the form of contact binary grains, but smaller grains can be present in the form of mixed grains.

Figure 2 shows the disruption grain size (also maximum size) as a function of the radiation strength U for the different gas densities and various ratio of two spherical grains s . The disruption size decreases rapidly with increasing U , but it increases with increasing the gas density due to enhanced gas damping. At large U , the disruption size becomes weakly depends on the gas density due to the dominance of infrared emission damping.

4.2. Composite model

A spherical dust grain of radius a rotating at velocity ω develops a tensile stress due to centrifugal force which scales as

$$S = \frac{\rho a^2 \omega^2}{4}. \quad (26)$$

When the rotation rate is sufficiently high such as the tensile stress exceeds the maximum limit, namely tensile strength S_{max} , the grain is disrupted. The critical

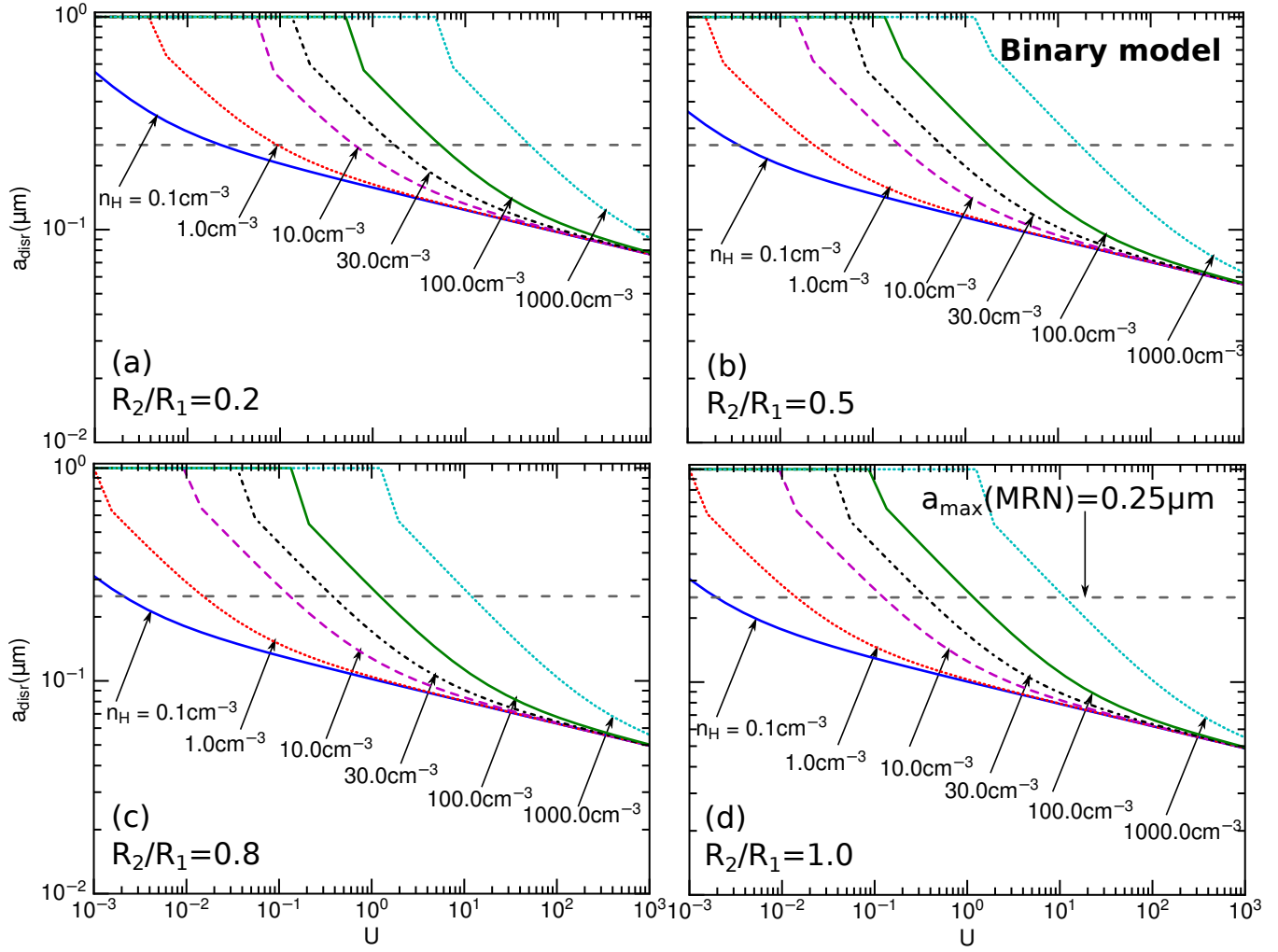


Figure 2. Disruption grain size of a contact binary model as a function of the radiation strength for the different gas density n_H , and we set $a_{\text{disr}} = 1.0 \mu\text{m}$ in case of no disruption. Four different values of the size ratio $s = R_2/R_1$ are considered. Horizontal dashed lines show the cutoff in MRN distribution of $a_{\text{max}} = 0.25 \mu\text{m}$.

Table 1. Maximum grain size for contact binary grain model

Gas density $n_H(\text{cm}^{-3})$	$a_{\text{disr}}(\mu\text{m})$				
	$U=0.1$	$U=1$	$U=10$	$U=10^2$	$U=10^3$
0.1	0.129	0.101	0.079	0.062	0.049
1.0	0.147	0.103	0.079	0.062	0.049
10	0.273	0.125	0.082	0.063	0.049
30	0.436	0.167	0.089	0.063	0.049
100	ND	0.267	0.111	0.067	0.049
1000	ND	ND	0.264	0.102	0.055

Notes: $R_2/R_1 = 1$.
ND= No Disruption

rotational velocity is given by $S = S_{\text{max}}$:

$$\omega_{\text{disr}} = \frac{2}{a} \left(\frac{S_{\text{max}}}{\rho} \right)^{1/2} \simeq \frac{3.6 \times 10^8}{a_{-5}} S_{\text{max},7}^{1/2} \hat{\rho}^{-1/2} \text{ rad s}^{-1}, \quad (27)$$

where $S_{\text{max},7} = S_{\text{max}}/10^7 \text{ erg cm}^{-3}$ (Draine & Lazarian 1998; Hoang et al. 2018a).

For strong radiation fields such that $F_{\text{IR}} \gg 1$, from Equations (18) and (27), one can obtain the disruption grain size:

$$\left(\frac{a_{\text{disr}}}{0.1 \mu\text{m}} \right)^{2.7} \simeq 5.1 \gamma_{\text{rad},-1}^{-1} U^{-1/3} \bar{\lambda}_{0.5}^{1.7} S_{\text{max},7}^{1/2}, \quad (28)$$

for $a_{\text{max}} \leq \bar{\lambda}/1.8$.

Table 2. Maximum grain size for composite grain model

Gas density $n_H(\text{cm}^{-3})$	$a_{\text{disr}}(\mu\text{m})$				
	$U=0.1$	$U=1$	$U=10$	$U=10^2$	$U=10^3$
0.1	0.159	0.117	0.088	0.066	0.049
1.0	0.190	0.121	0.088	0.066	0.049
10	0.458	0.159	0.093	0.067	0.049
30	ND	0.239	0.104	0.068	0.050
100	ND	0.450	0.139	0.072	0.051
1000	ND	ND	0.4465	0.127	0.058

^c $a_p = 5\text{nm}$, $S_{\text{max}} \sim 10^6 \text{ erg cm}^{-3}$

Table 3. Maximum grain size for core-mantle grain model

Gas density $n_H(\text{cm}^{-3})$	$a_{\text{disr}}(\mu\text{m})$ ^a				
	$U=0.1$	$U=1$	$U=10$	$U=10^2$	$U=10^3$
0.1	0.235	0.1719	0.129	0.097	0.073
1.0	0.302	0.1801	0.129	0.097	0.073
10	ND	0.262	0.139	0.098	0.073
30	ND	0.422	0.162	0.101	0.073
100	ND	ND	0.237	0.110	0.074
1000	ND	ND	ND	0.223	0.089

^a Results obtained for $S_{\text{max}} = 10^7 \text{ erg cm}^{-3}$

For an arbitrary radiation field, one obtains

$$\left(\frac{a_{\text{disr}}}{0.1 \mu\text{m}}\right)^{1.7} \simeq 11.4 \gamma_{\text{rad}, -1}^{-1} U^{-1} \bar{\lambda}_{0.5}^{1.7} S_{\text{max}, 7}^{1/2} \times \left(\frac{1 + F_{\text{IR}}}{\hat{n}^{-1} \hat{T}_{\text{gas}}^{-1/2}}\right), \quad (29)$$

which depends on the local gas density and temperature due to gas damping.

Table 1 shows the disruption size for the different radiation strengths and gas density, assuming the particle radius $a_p = 5 \text{ nm}$ as in Mathis & Whiffen (1989).

Figure 3 shows the disruption size as a function of U for the different values of particle radius. The disruption size decreases significantly with increasing the particle radius a_p due to the lower tensile strength. Increasing the gas density results in an increase in the disruption size due to the effect of gas collisional damping. For the typical ISM and $U = 1$, the disruption size is $a_{\text{disr}} \approx 0.1 \mu\text{m}$ for the particle radius $a_p \sim 25 \text{ nm}$.

4.3. Core-mantle model

We assume that the ice mantle is thick enough such that it can behaves like bulk ice. Therefore, the disruption of the core-mantle grain is not different from a compact grain, except the fact that in the later, the only mantle layer is ejected by the centrifugal force. The disruption size can be calculated by Equation (28) and (29) for $S_{\text{max}} = 10^7 \text{ erg cm}^{-3}$.

Table 3 shows the disruption size for core-mantle grains. Results for compact grains with $S_{\text{max}} = 10^9 \text{ erg cm}^{-3}$ are also shown for comparison.

Figure 3 shows the disruption size for the different gas density for a core-mantle grain (left panel) and compact grain (right panel). Same trend as Figures 2 and 3 are seen.

5. DISCUSSION

5.1. Why do we need dynamical constraints for dust models?

Interstellar dust models are usually construed using observational constraints from starlight extinction and polarization (see Draine 2003). By varying the grain size distribution, a large number of dust models can successfully reproduce observational data (Zubko et al. 2004), including compact grains (Weingartner & Draine 2001), composite (Mathis 1996), and core-mantle models (Li & Greenberg 1997). As a consequence, one cannot get insight into internal structures of dust grains because a variety of grain models with different internal structures reproduce well observational data. In the light of a recent discovery by Hoang et al. (2018b) that centrifugal force due to suprathermal rotation induced by RATs can disrupt large grains, in this paper, we showed that rotational disruption is an important dynamical constraint of dust models (i.e., grain size distribution), and this dynamical constraint can pave the way for probing internal structures of grains using observations.

Table 4 shows the disruption size by RATD for the different grain models, including binary, composite, and core-mantle models. Compact grains are not affected by the dynamical constraint if the radiation field is $U \leq 1$, but all other models have the maximum size below $0.5 \mu\text{m}$. Composite grains of tiny particles of $a_p \sim 5 \text{ nm}$ can survive in the ISRF if their size is below $0.25 \mu\text{m}$. For larger inclusions of $a_p \sim 25 \text{ nm}$ which have smaller tensile strength, large composite grains ($a > 0.1 \mu\text{m}$) cannot survive because of disruption. As the radiation strength U increases, the disruption size is decreased due to stronger RATD efficiency.

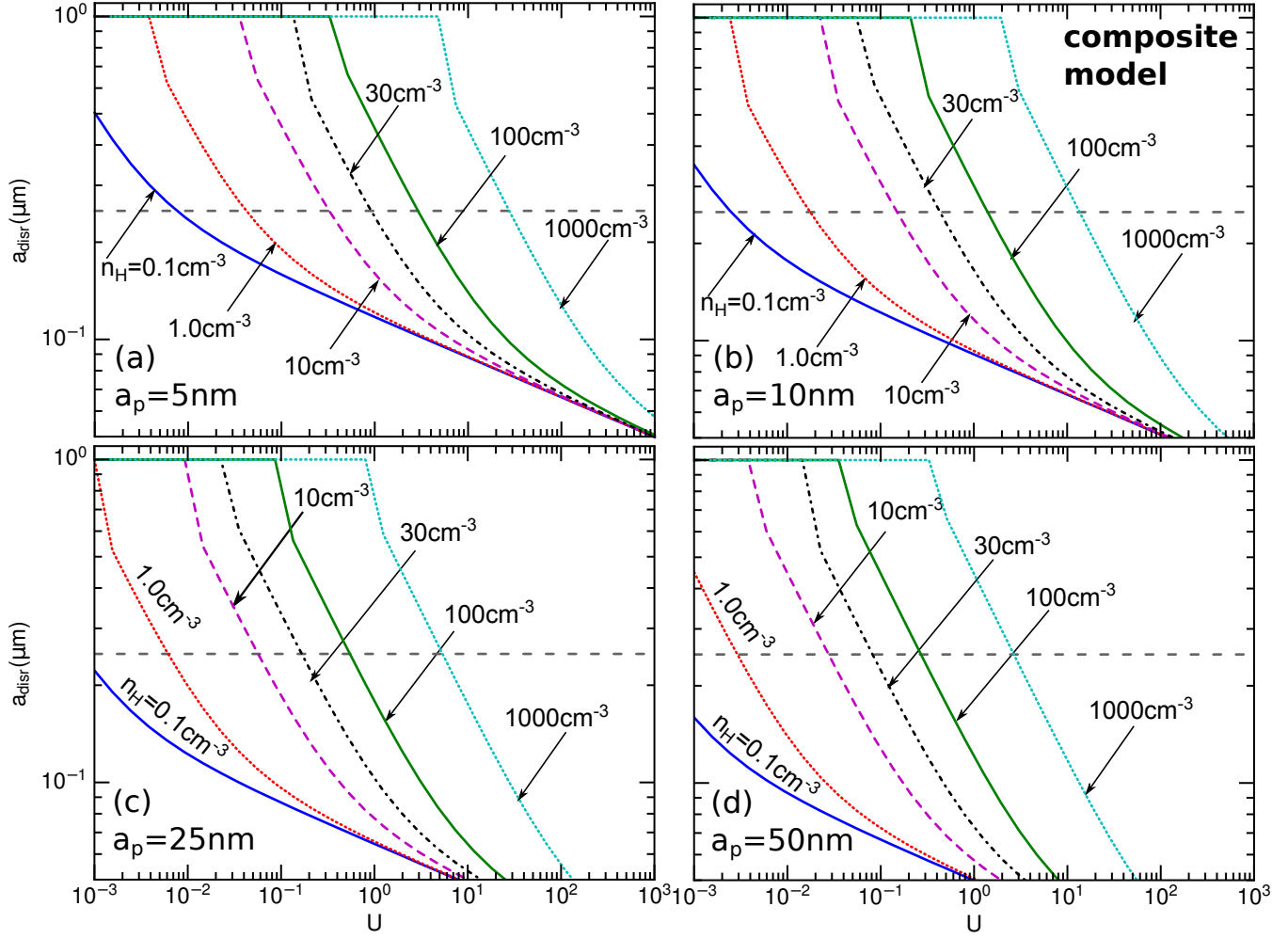


Figure 3. Same as Figure 2 but for a composite grain model with porosity $P = 0.2$ and different particle radius a_p . The particle radius and its corresponding tensile strength are shown.

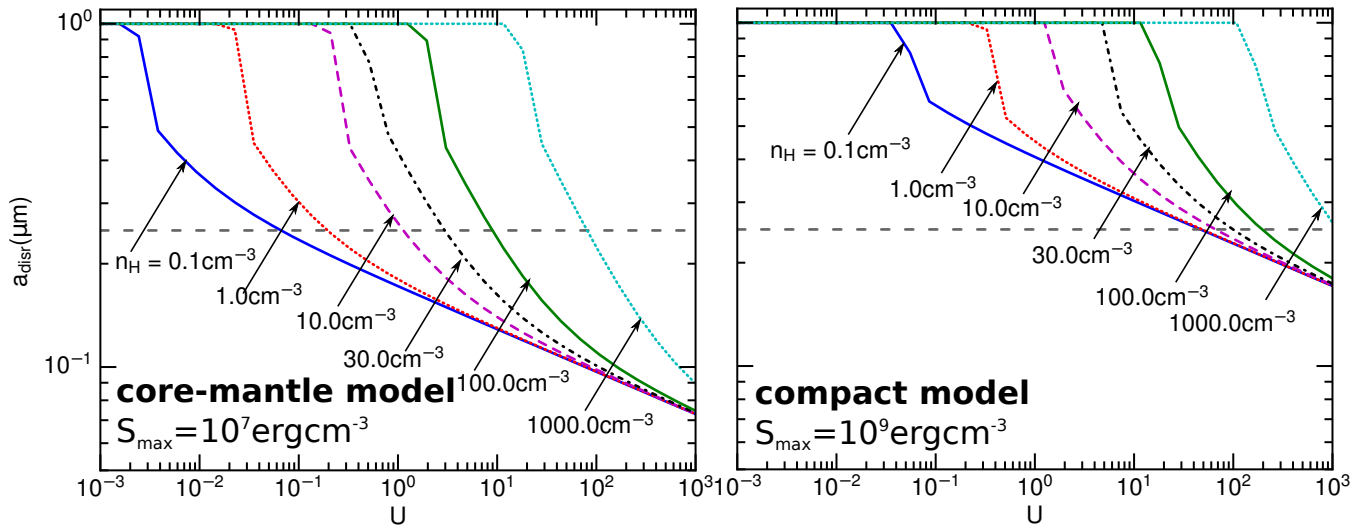


Figure 4. Disruption size for core-mantle grain models with $S_{\text{max}} = 10^7 \text{erg cm}^{-3}$ (left panel) and 10^9erg cm^{-3} (right panel).

Table 4. Maximum grain size for different dust models in the diffuse ISM

Grain Model	$a_{\text{disr}} (\mu\text{m})$				
	U=0.1	U=1	U=10	U=10 ²	U=10 ³
Binary ^a	0.523	0.198	0.102	0.072	0.055
Binary ^b	0.436	0.167	0.089	0.063	0.049
Composite ^c	ND	0.239	0.103	0.068	0.050
Composite ^d	0.333	0.102	0.053	0.037	0.027
Core-mantle ^e	ND	0.421	0.162	0.100	0.073
Compact ^f	ND	ND	0.484	0.249	0.174

Notes: Diffuse ISM of $n_{\text{H}} = 30 \text{ cm}^{-3}$, $T_{\text{gas}} = 100\text{K}$.

^a $R_2/R_1 = 0.5$; ^b $R_2/R_1 = 1$

^c $a_p = 5 \text{ nm}$, $S_{\text{max}} = 1.2 \times 10^6 \text{ erg cm}^{-3}$

^d $a_p = 25 \text{ nm}$, $S_{\text{max}} = 5.1 \times 10^4 \text{ erg cm}^{-3}$

^e $S_{\text{max}} = 10^7 \text{ erg cm}^{-3}$

^f $S_{\text{max}} = 10^9 \text{ erg cm}^{-3}$

One note that, the RATD occurs on a timescale:

$$t_{\text{disr}} = \frac{I\omega_{\text{disr}}}{dJ/dt} = \frac{I\omega_{\text{disr}}}{\Gamma_{\text{RAT}}}, \quad (30)$$

$$\simeq 10^5 U^{-1} \bar{\lambda}_{0.5}^{1.7} S_{\text{max},7}^{1/2} \left(\frac{a_{\text{disr}}}{0.1 \mu\text{m}} \right)^{-0.7} \text{ yr}, \quad (31)$$

which is much shorter than the shattering time by grain-grain collisions:

$$\tau_{\text{shat}} = \frac{1}{\pi a^2 n_{\text{gr}} v_{\text{gg}}} = \frac{4\rho a}{3n_{\text{H}} m_{\text{H}} v_{\text{gg}}},$$

$$\simeq 2.5 \times 10^5 a_{-5} \left(\frac{30 \text{ cm}^{-3}}{n_{\text{H}}} \right) \left(\frac{1 \text{ km s}^{-1}}{v_{\text{gg}}} \right) \text{ yr}, \quad (32)$$

where we assume the single size a distribution with the gas-to-dust mass ratio of 100 and the grain density n_{gr} , and v_{gg} is the relative velocity of grains.

Therefore, RATD can play an important role in constraining the maximum grain size of grains in the diffuse ISM, which is thought due to grain shattering (Hirashita & Yan 2009) induced by grain acceleration in magnetohydrodynamic (MHD) turbulence (Yan et al. 2004; Hoang et al. 2012). Because the RATD depends on the tensile strength of the grain, local gas properties and radiation field, the upper cutoff a_{max} is different for the different grain models and changes with the local conditions.

5.2. Constraining grain internal structures with observations

One of the mystery of interstellar dust is the internal structure of dust grains, such as how constituents are organized. To date, no theoretical attempt have been made to relate the grain internal structure with observable.

Here we suggest that the RATD effect can be used to constrain the internal structure because the RATD efficiency depends on the grain tensile strength which is characterized by the grain structure and compositions. Our strategy is as follows. First, using observational constraints of extinction and polarization one can obtain the maximum grain size a_{max} . By comparing a_{max} with the disruption size a_{disr} , one then can constrain the tensile strength of grains. This can provide insight into whether grains are compact/core-mantle or composite. If the grain is composite, then, one can further infer the average radius of individual particles a_p and porosity.

The first potential scenario is to observe RATD in strong radiation fields such as supernovae and novae. Our estimates in Hoang et al. (2018b) show the maximum grain size decreases with the decreasing the cloud distance to the supernova. If the cloud distance can be estimated such as through time evolution of color excess (Bulla et al. 2018b; Bulla et al. 2018a), one can then obtain the tensile strength by comparing the disruption size with the grain size estimated from reddening observations.

The second scenario is to use polarimetric observations. Indeed, the largest grains dominate the emission and polarization at long, far-infrared/submm wavelengths. Therefore, in the RAT alignment paradigm, the degree of far-IR/submm polarization first increases with increasing the radiation strength and then declines beyond some critical strength due to RATD. Interestingly, this trend might already be seen in Planck data (Collaboration et al. 2018).

5.3. Are silicate and carbonaceous grains really separate?

Chiar et al. (2006) found that the $3.4 \mu\text{m}$ C-H feature is negligibly polarized, whereas the $9.7 \mu\text{m}$ Si-O feature is strongly polarized for the light of sights toward the Galactic Center. The authors suggest that carbonaceous grains must be a separate component and these grains should be not aligned. Theoretically, if carbon grains are separate, they cannot be aligned due to their diamagnetic nature (Hoang & Lazarian 2016). The question now is why there are two separate silicate and carbonaceous materials?

Using our results in Section 4, we show that large composite grains ($a > 0.1 \mu\text{m}$) with the particle radius $a_p > 25 \text{ nm}$ are not stable in the ISM due to the low tensile strength, but composite grains with $a_p < 10 \text{ nm}$ can survive RATD if their size is below $0.3 \mu\text{m}$ (see Table

4). Therefore, if the original silicate and carbon grains are typically sized above ~ 50 nm, then, the sticking collisions of these particles will form a composite grain, which is rapidly destroyed by RATD.

Moreover, carbon material can be mixed with silicate grains through contact binary or core-mantle models. For both models, large mixed grains can withstand the RATD. Nevertheless, if the mantle is much thinner than the core radius, then, the $3.4 \mu\text{m}$ feature is absent from core-mantle grain, which can explain the negligible polarization of $3.4 \mu\text{m}$ feature (Jones et al. 2013; see Jones 2016 for a review). An alternative explanation is that the average radiation along the line of sight toward GC is significantly enhanced such that RATD can disrupt all mixed grains, including composite and core and mantle.

Finally, one note that in molecular clouds, RATD is inefficient due to weak radiation fields and high gas density. As a result, large mixed silicate-carbonaceous grains can be present. This prediction would be tested with polarimetric observations.

6. SUMMARY

Using the RATD effect discovered by Hoang et al. (2018b), we have introduced a new dynamical constraint for interstellar dust models and studied implications of this constraint. The main results are summarized as follows:

- For all dust models except compact grains, we find that large grains of size $a > 0.45 \mu\text{m}$ are destroyed by RATD in the average ISRF (i.e., $U = 1$). Stronger radiation fields result in the disruption of smaller grains.
- For the composite model, we find that large com-

posite grains made of small individual particles of radius $a_p \leq 25\text{nm}$ can survive in the average ISRF with the upper limit of $a_{\text{max}} \sim 0.24 \mu\text{m}$, which is incidentally similar to the upper cutoff of MRN distribution. The maximum size decreases to $a_{\text{max}} \sim 0.1 \mu\text{m}$ for $U = 10$. As a result, large composite grains can survive in the diffuse ISM.

- The growth of grains toward micron size in the diffuse ISM would be prohibited by RATD, but it would proceed in weak radiation fields such as dense molecular clouds.
- We explain the non-detection of polarization at the $3.4 \mu\text{m}$ C-H feature by means of two separate silicate and carbonaceous dust materials which are disrupted by RATs from original composite grains made of large individual particles of radius $a_p \geq 50$ nm.
- Using RATD effect, we suggest that internal structures of grains can be constrained by observations of starlight extinction and polarization for the conditions with varying radiation fields, such as in the vicinity of a star, supernovae, and novae.

T.H thanks B.T Draine, A. Lazarian, and V. Guillet for discussions on various issues related to radiative torque disruption and its application. This work was supported by the Basic Science Research Program through the National Research Foundation of Korea (NRF), funded by the Ministry of Education (2017R1D1A1B03035359).

REFERENCES

- Aitken, D. K., Smith, C. H., James, S. D., Roche, P. F., & Hough, J. H. 1988, *MNRAS*, 230, 629
- Bethell, T. J., Chepurnov, A., Lazarian, A., & Kim, J. 2007, *ApJ*, 663, 1055
- Bulla, M., Goobar, A., Amanullah, R., Feindt, U., & Ferretti, R. 2018a, *MNRAS*, 473, 1918
- Bulla, M., Goobar, A., & Dhawan, S. 2018b, *MNRAS*, 479, 3663
- Chiar, J. E., Adamson, A. J., Whittet, D. C. B., et al. 2006, *ApJ*, 651, 268
- Chokshi, A., Tielens, A. G. G. M., & Hollenbach, D. 1993, *ApJ*, 407, 806
- Collaboration, P., Aghanim, N., Akrami, Y., Alves, M. I. R., & et al. 2018, *arXiv.org*
- Dominik, C., & Tielens, A. G. G. M. 1997, *The Astrophysical Journal*, 480, 647
- Draine, B. T. 2003, *ARA&A*, 41, 241
- Draine, B. T., & Fraise, A. A. 2009, *ApJ*, 696, 1
- Draine, B. T., & Lazarian, A. 1998, *ApJ*, 508, 157
- Draine, B. T., & Lee, H. M. 1984, *ApJ*, 285, 89
- Draine, B. T., & Li, A. 2007, *ApJ*, 657, 810
- Draine, B. T., & Weingartner, J. C. 1996, *ApJ*, 470, 551
- Greenberg, J. M., & Li, A. 1996, *Astronomy and Astrophysics*, 309, 258
- Greenberg, J. M., Mizutani, H., & Yamamoto, T. 1995, *A&A*, 295, L35
- Guhathakurta, P., & Draine, B. T. 1989, *ApJ*, 345, 230
- Guillet, V., Fanciullo, L., Verstraete, L., et al. 2017, *A&A*
- Heim, L.-O., Blum, J., Preuss, M., & Butt, H.-J. 1999, *Physical Review Letters*, 83, 3328
- Hensley, B. S., & Bull, P. 2018, *The Astrophysical Journal*, 853, 127
- Herranen, J., Lazarian, A., & Hoang, T. 2018, *arXiv:1812.07274*
- Hirashita, H., & Yan, H. 2009, *MNRAS*, 394, 1061
- Hoang, T. 2017, *ApJ*, 836, 13
- Hoang, T., Draine, B. T., & Lazarian, A. 2010, *ApJ*, 715, 1462
- Hoang, T., & Lazarian, A. 2008, *MNRAS*, 388, 117
- Hoang, T., & Lazarian, A. 2009, *ApJ*, 695, 1457
- Hoang, T., & Lazarian, A. 2014, *MNRAS*, 438, 680
- Hoang, T., & Lazarian, A. 2016, *ApJ*, 831, 159
- Hoang, T., Lazarian, A., & Draine, B. T. 2011, *ApJ*, 741, 87

- Hoang, T., Lazarian, A., & Schlickeiser, R. 2012, *ApJ*, 747, 54
- Hoang, T., Loeb, A., Lazarian, A., & Cho, J. 2018a, *ApJ*, 860, 0
- Hoang, T., & Tram, L. N. 2018, arXiv:1810.12007
- Hoang, T., Tram, L. N., Lee, H., & Ahn, S.-H. 2018b, arXiv:1810.05557
- Johnson, K. L., Kendall, K., & Roberts, A. D. 1971, in *Proceedings of the Royal Society of London. Series A*, 301–313
- Jones, A. P. 2016, *Royal Society Open Science*, 3, 160224
- Jones, A. P., Fanciullo, L., Köhler, M., et al. 2013, *Astronomy and Astrophysics*, 558, 62
- Kamionkowski, M., & Kovetz, E. D. 2016, *ARA& A*, 54, 227
- Kim, S.-H., Martin, P. G., & Hendry, P. D. 1994, *ApJ*, 422, 164
- Lazarian, A., & Hoang, T. 2007, *MNRAS*, 378, 910
- Li, A., & Greenberg, J. M. 1997, *A&A*, 323, 566
- Litwin, K. L., Zygielbaum, B. R., Polito, P. J., Sklar, L. S., & Collins, G. C. 2012, *Journal of Geophysical Research: Planets*, 117, n/a
- Mathis, J. S. 1996, *ApJ*, 472, 643
- Mathis, J. S., Mezger, P. G., & Panagia, N. 1983, *A&A*, 128, 212
- Mathis, J. S., Rumpl, W., & Nordsieck, K. H. 1977, *ApJ*, 217, 425
- Mathis, J. S., & Whiffen, G. 1989, *ApJ*, 341, 808
- Weingartner, J. C., & Draine, B. T. 2001, *ApJ*, 548, 296
- Yan, H., Lazarian, A., & Draine, B. T. 2004, *ApJ*, 616, 895
- Zubko, V., Dwek, E., & Arendt, R. G. 2004, *ApJS*, 152, 211